University of Massachusetts Amherst

From the SelectedWorks of Derek Lovley

January 16, 2012

Biofilm conductivity is a decisive variable for high-current-density Geobacter sulfurreducens microbial fuel cells

Nikhil S. Malvankar, *University of Massachusetts - Amherst*
Mark T. Tuominen, *University of Massachusetts - Amherst*
Derek Lovley, *University of Massachusetts - Amherst*

Available at: https://works.bepress.com/derek_lovley/375/

View Article Online / Journal Homepage / Table of Contents for this issue
Dynamic Article Links

Energy & Environmental Science

Cite this: *Energy Environ. Sci.*, 2012, **5**, 5790

www.rsc.org/ees

PAPER

Biofilm conductivity is a decisive variable for high-current-density *Geobacter sulfurreducens* microbial fuel cells

Nikhil S. Malvankar,*[ab] Mark T. Tuominen[a] and Derek R. Lovley[b]

Received 6th December 2011, Accepted 20th December 2011
DOI: 10.1039/c2ee03388g

Downloaded by University of Massachusetts - Amherst on 12 March 2013
Published on 16 January 2012 on http://pubs.rsc.org | doi:10.1039/C2EE03388G

Current outputs of microbial fuel cells (MFCs) are too low for most perceived practical applications. Most efforts for further optimization have focused on modifications of fuel cell architecture or electrode materials, with little investigation into the properties of microorganisms that are most essential for maximal current production. *Geobacter sulfurreducens* produces the highest current densities of any known pure culture; is closely related to the *Geobacter* species that often predominate in anode biofilms harvesting electricity from organic wastes; and produces highly conductive anode biofilms. Comparison of biofilm conductivities and current production in different strains of *G. sulfurreducens* revealed a direct correlation between biofilm conductivity and current density. Electrochemical impedance spectroscopy measurements demonstrated that higher biofilm conductivity not only reduced resistance to electron flow through the biofilm, but also lowered the activation energy barrier for electron transfer between the biofilm and the anode. These results demonstrate the crucial role of biofilm conductivity in achieving high current density in MFCs and suggest that increasing biofilm conductivity can boost MFC performance.

Introduction

Although microbial fuel cells show promise as a strategy for converting waste organic matter to electricity, low power outputs have limited practical applications.[1,2] Most efforts to develop improved microbial fuel cells have focused on engineering better fuel cell architecture and/or materials with the implicit assumption that the current-production capacity of the microorganisms is fixed.

However, there probably has been little selective pressure on microorganisms for optimal current production because the ability to produce current is most likely fortuitous, resulting from adaption for extracellular electron transfer to insoluble Fe(III) oxides.[1] Thus, there may be significant opportunities to increase the current-producing capacity of microorganisms, if the biological factors limiting current production can be determined.

Geobacter sulfurreducens produces the highest current densities of any microorganism available in pure culture[3,4] and microorganisms closely related to *G. sulfurreducens* are often enriched on

[a]*Department of Physics, University of Massachusetts, Amherst, MA, USA. E-mail: nikhil@physics.umass.edu; Fax: +413-577-4660; Tel: +413-577-1391*
[b]*Department of Microbiology, University of Massachusetts, Amherst, MA, USA*

Broader context

The microbial fuel cell (MFC) is an emergent technology for efficient conversion of organic wastes into electricity. MFCs have significant potential for powering electronic devices in remote areas such as sea-floors and for removing organic pollutants from wastewater while producing electricity. A key component of MFCs is the biofilm of microorganisms that grows on the anode, oxidizing organic compounds with electron transfer to the anode. Although most commonly studied biofilms are electronically insulating, biofilms of the current-producing microbe *Geobacter sulfurreducens* exhibit electronic conductivity rivaling to those of synthetic conducting polymers. The observed metallic-like conductivity is associated with a network of microbial nanowires coursing through the biofilms. Extracellular electron transfer *via* a conductive biofilm has been suggested as the most efficient mechanism for high-current density MFCs. Here we experimentally demonstrate for the first time a direct correlation between biofilm conductivity and current production. We show that increased biofilm conductivity reduces potential losses and internal resistance of MFCs, enabling enhanced current density. Our studies reveal that biofilm conductivity is an integral part of the extracellular electron transport chain of *G. sulfurreducens*, facilitating electron transfer to electrodes. The results suggest that increasing the biofilm conductivity can be an effective strategy to maximize MFC performance.

This journal is © The Royal Society of Chemistry 2012

Published on 16 January 2012 on http://pubs.rsc.org | doi:10.1039/C2EE03388G
Downloaded by University of Massachusetts - Amherst on 12 March 2013

anodes from mixed microbial communities, especially in fuel cells operating at high current densities, with high coulombic efficiency.[5–7]

The ability of *G. sulfurreducens* to produce highly conductive biofilms[9] may be an important factor contributing to its ability to generate high current densities. Although previous studies have speculated that the biofilm conductivity can be attributed to electron hopping between *c*-type cytochromes,[10,11] this model is inconsistent with multiple lines of evidence, including the temperature-dependence of the biofilm conductivity and the localization of the cytochromes.[12] The preponderance of evidence suggests that the conductivity through *G. sulfurreducens* biofilms can be attributed to a network of electrically conductive pili, known as microbial nanowires,[9,13] that transport electrons over long distances with metallic-like conductivity.[9] A similar conductivity has been directly measured in methanogenic aggregates[14] as well as in current-producing biofilms developed from anaerobic wastewater digesters.[15] Furthermore, modeling of similar current-producing biofilms demonstrated that it was necessary to invoke biofilm conductivity in order to describe current production.[10,16–21] *Geobacter* species were important components of all these systems.

In non-biological systems increasing the conductivity of the catalytic layer on electrodes increases current density.[22] However, there is uncertainity in the literature over whether biofilm conductivity is an important factor limiting current production in microbial fuel cells. Modeling studies suggested that a higher biofilm conductivity can enhance the fuel cell current density.[16] In contrast, some studies based on experimental work concluded that biofilm conductivity does not limit current density,[10,20,21] whereas other studies[18,19] have suggested that biofilm conductivity can limit the amount of current-producing biomass that can grow on an anode. However, in all those studies, conductivity was not measured directly, but only inferred from indirect evidence.

The purpose of the studies reported here was to compare the current production of strains of *G. sulfurreducens* with different biofilm conductivities. The results demonstrate a direct correspondence between biofilm conductivity and fuel cell current density and reveal the crucial role of biofilm conductivity in achieving high current density in microbial fuel cells.

Results and discussion

Biofilm conductivity is an important factor in the high-performance *Geobacter sulfurreducens* microbial fuel cells

Given the doubt about the relationship between biofilm conductivity and the capacity for current production that has arisen from indirect inference of biofilm conductivity, biofilm conductivity was directly measured in strains of *G. sulfurreducens* that produced different current densities. Strains of *G. sulfurreducens* that produced biofilms with higher conductivities produced higher current densities in microbial fuel cells (Fig. 1). For example, previous studies[9] demonstrated that the biofilms of strain KN400, a strain selected for higher current production,[4] were more highly conductive than strain DL-1, the most commonly studied strain of *G. sulfurreducens* and, consistent with previous reports,[4] KN400 produced higher current densities than DL-1 (Fig. 1).

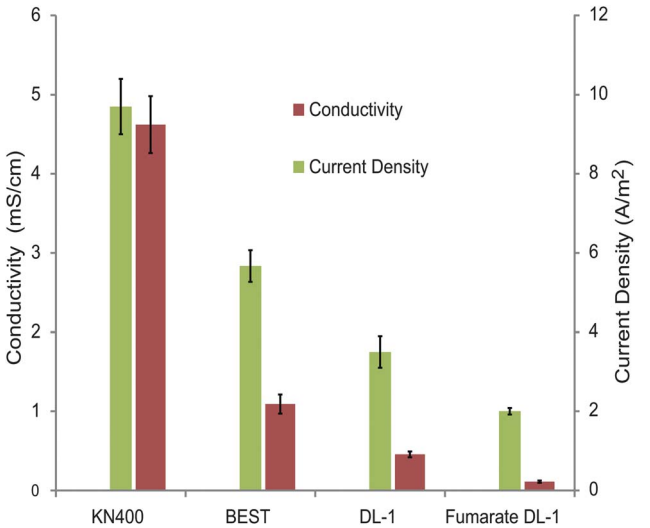

Fig. 1 Correlation between biofilm conductivity and fuel cell current density for biofilms of strains KN400 and DL-1,[4] strain Fumarate DL-1[8] and for strain BEST (this study). Bars represent mean ± standard deviation for biological replicates.

The BEST strain[23] was generated by deleting the genes for the outer-surface cytochromes OmcB, OmcE, OmcS, and OmcT from strain DL-1. Strain BEST had biofilm conductivities intermediate between that of DL-1 and KN400 and current production also fell between that of KN400 and DL-1 (Fig. 1). Biofilms of strain DL-1 can be grown on electrode surfaces that are not connected to a cathode if the alternative electron acceptor fumarate is provided as an electron acceptor.[8] These fumarate-grown biofilms are less conductive than biofilms of DL-1 grown with an electrode as the electron acceptor[9] and produced less current than electrode-grown biofilms when an electrical connection was made with a cathode (Fig. 1).[8]

There was a strong correlation ($r^2 = 0.96$) between biofilm conductivity and the fuel cell current density of the different *G. sulfurreducens* strains, indicating that biofilm conductivity plays a central role in long-range electron transport to the anode and that the capacity to produce biofilms with more conductivity directly translates into higher fuel cell current densities.

Biofilm conductivity is sufficient for observed current production

If long-range electron transport through conductive biofilms is the mechanism by which cells at a distance from the anode are transferring electrons to the anode, then the conductivity of the biofilm must be sufficient to account for known rates of electron transfer. The electron transfer rate of *Geobacter sulfurreducens* on soluble electron acceptors and on electrodes has been reported to be *ca.* 5×10^{16} electrons per second per mg protein.[24,25] For strain DL-1, the protein concentration in the gap was *ca.* 30 μg. The potential difference between the electron donor acetate (−500 mV *vs.* Ag/AgCl) and the anode (−400 mV *vs.* Ag/AgCl as measured in our setup) is 100 mV. The electron transport rate (Γ) was computed using the relation $\Gamma = I/e$ where I is the measured current and e is the electron charge. With the measured biofilm

Published on 16 January 2012 on http://pubs.rsc.org | doi:10.1039/C2EE03388G
Downloaded by University of Massachusetts - Amherst on 12 March 2013

conductivity of *ca.* 0.5 mS cm^{-1}, this yields an electron transport rate *ca.* 1×10^{16} electrons per second per mg protein at 100 mV of applied bias, which compares favorably with the previously reported[24,25] electron transfer rate of *G. sulfurreducens* and suggests that the conductivity of the biofilm is sufficient to account for observed levels of current production.

The measurements described above were made on biofilms spanning non-conducting gaps of 50 μm. It was recently suggested that *G. sulfurreducens* lacks sufficient conductivity to bridge 100 μm gaps.[19] If so, this could be an important consideration in evaluating current production capabilities. However, biofilms of strain DL-1 bridged 100 μm gaps (Fig. 2A) with conductance values comparable to the measurements across the 50 μm gap (Fig. 2B). As expected, the biofilm took a longer time to bridge the larger, 100 μm, gap than to bridge the smaller, 50 μm, gap. The previously reported[19] inability of *G. sulfurreducens* biofilm to span a 100 μm gap might be due to the small width (10 μm) of the electrodes employed, or might be attributed to the fact that the biofilms were visualized with scanning electron microscopy. Although confocal images clearly showed that the gap was bridged (Fig. 2A), SEM images failed to show the filling of the gap by the biofilm; which is presumably due to biofilm disruption in the fixation process (Fig. 3).

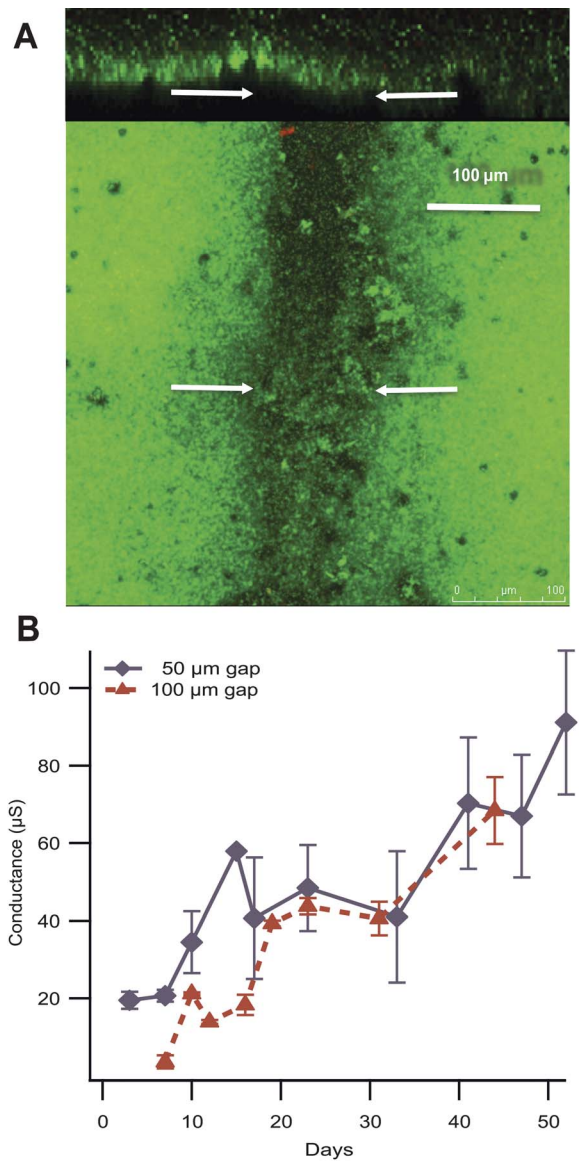

Fig. 2 (A) Confocal image of the biofilm filling the 100 μm non-conductive gap across gold electrodes. Gap is designated by arrows. Scale bar 100 μm. (B) Comparison of biofilm conductance across 50 μm and 100 μm gaps. Error bars represent one standard deviation.

Increased biofilm conductivity also lowers the resistance for electron transfer between the biofilm and the anode

The resistance for electron flow through anode biofilms is just one of many potential electron transfer steps that can limit the current output of microbial fuel cells (Fig. 4). Each electron transfer step results in electric potential losses,[17,26] contributing to the total internal resistance. These multiple components (Fig. 4) can be defined as:[27,28]

$$R_{int} = R_{ct}^{anode} + R_{ct}^{cathode} + R_{\Omega} \quad (1)$$

where R_{ct}^{anode} and $R_{ct}^{cathode}$ are the charge transfer (polarization) resistance for the anode and cathode respectively and R_{Ω} contains ohmic contributions. R_{Ω} can be further broken down into the following components:

$$R_{\Omega} = R_{anolyte} + R_{catholyte} + R_{membrane} + R_{Biofilm} \quad (2)$$

where $R_{anolyte}$ and $R_{catholyte}$ are electrolyte resistances at the anode and cathode, respectively; $R_{membrane}$ is the resistance associated with the proton exchange membrane (PEM, Fig. 4) and $R_{biofilm}$ is the resistance to electron flow through the biofilm. From these considerations it is apparent that, if all other resistances remain constant, then increasing biofilm conductivity (*i.e.* lowering $R_{Biofilm}$) should lower the overall internal resistance and increase current output.

In order to determine whether there were differences in any of the other resistances associated with differences in biofilm conductivity, the other resistance components of the *Geobacter* fuel cells were evaluated with electrochemical impedance

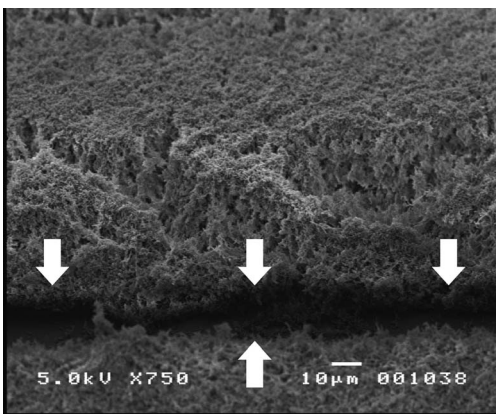

Fig. 3 Scanning electron microscopy (SEM) image of critical-point dried biofilm showing the cells not filling the non-conducting gap due to the artifacts of SEM sample preparation requirements. Gap is designated by arrows. Scale bar 10 μm.

This journal is © The Royal Society of Chemistry 2012

Downloaded by University of Massachusetts - Amherst on 12 March 2013
Published on 16 January 2012 on http://pubs.rsc.org | doi:10.1039/C2EE03388G

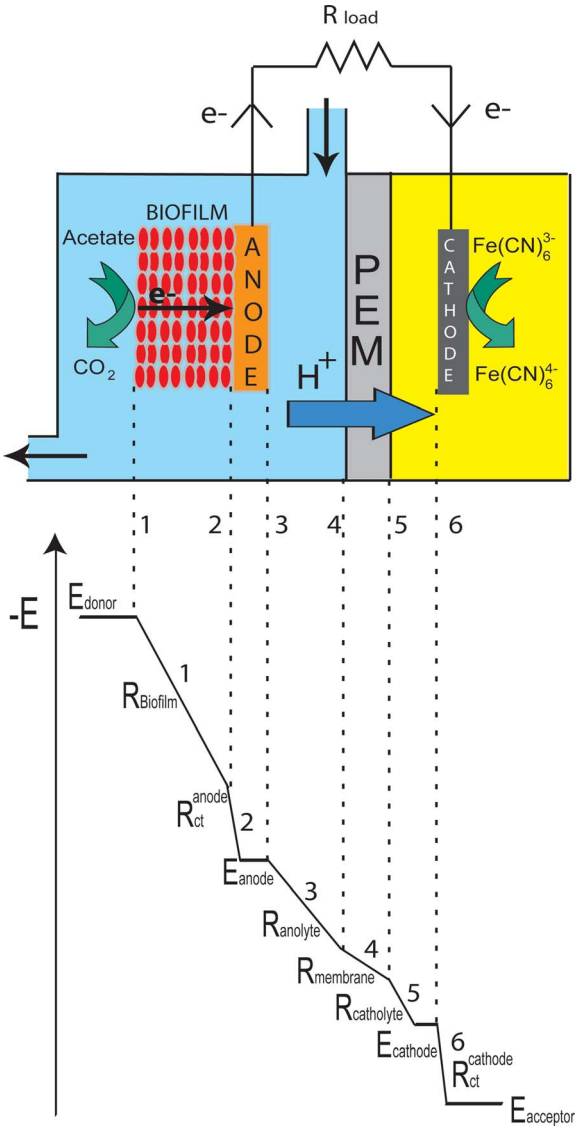

Fig. 4 Schematic of microbial fuel cell and potential losses associated with each electron transfer step: 1. Losses due to the biofilm resistance. 2. Losses due to the charge transfer resistance at anode. 3. Losses due to the anolyte. 4. Losses due to the proton exchange membrane (PEM). 5. Losses due to the catholyte. 6. Losses due to the charge transfer resistance at cathode. *E* is the potential and *R* is the resistance.

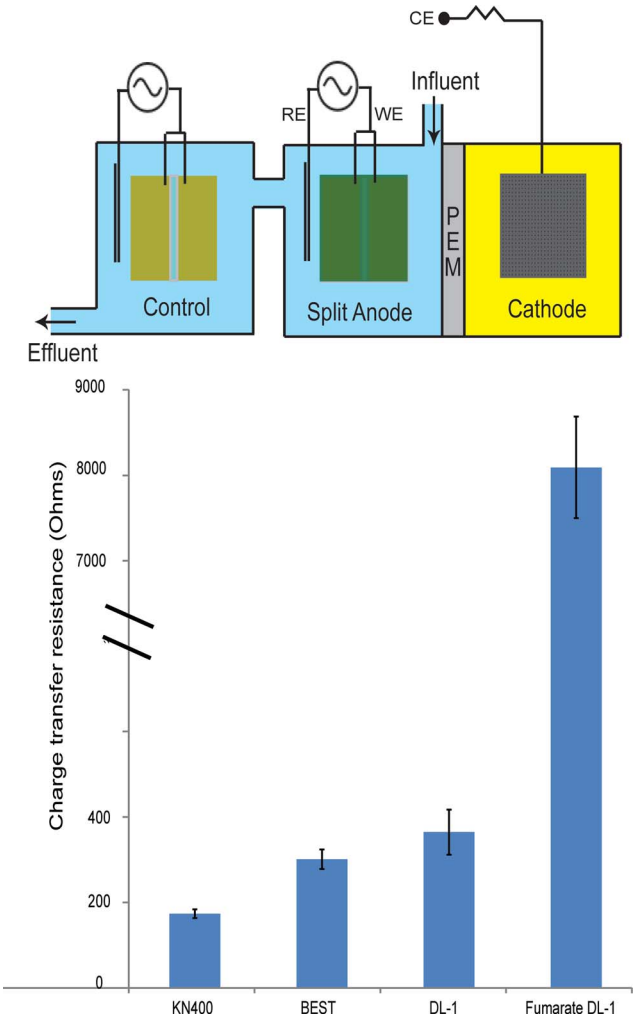

Fig. 5 (A) Setup for electrochemical impedance spectroscopy (EIS). RE: Reference electrode, WE: Working electrode and CE: Counter electrode (B) Higher conductive biofilms had lower charge transfer resistance. Strains are presented from left to right in decreasing order of biofilm conductivity. Error bars represent standard deviation.

spectroscopy (EIS) (Fig. 5A). R_{int} is equivalent to R_{ct}^{cell}, which is measurable as the dc limit of the impedance of the microbial fuel cell.[27] When the fuel cell design remains unchanged, $R_{anolyte}$, $R_{catholyte}$, and $R_{membrane}$ should remain constant. EIS measurements (Fig. 5 and 6) yielded following values: $R_{anolyte} = 14.3 \pm 0.3\ \Omega$, $R_{catholyte} = 0.36 \pm 0.01\ \Omega$ and $R_{\Omega}^{cell} = R_{anolyte} + R_{catholyte} + R_{membrane} = 35.1 \pm 0.3\ \Omega$. Therefore, $R_{membrane} = 20.44 \pm 0.6\ \Omega$. Additionally, $R_{ct}^{cathode} = 1.46 \pm 0.03\ \Omega$ and for the biofilm of DL-strain, $R_{ct}^{anode} = 356 \pm 52\ \Omega$ and $R_{ct}^{cell} = R_{int} = 1267 \pm 225\ \Omega$.

The strain of an organism at the anode is not expected to influence $R_{ct}^{cathode}$, which is only dependent on reactions at the cathode. EIS measurements yielded $R_{ct}^{cathode} \approx 1.5\ \Omega$. However, it is conceivable that the resistance for electron exchange between the biofilm and the anode, R_{ct}^{anode}, known as charge transfer resistance, might vary with the microbial strain because the charge transfer resistance arises from an activation energy barrier present at the biofilm-electrode interface.[27]

In order to evaluate whether the biofilm conductivity influences the electron transfer reaction at the biofilm/anode interface, simultaneous measurement of $R_{Biofilm}$ and R_{ct}^{anode} were performed on the same biofilm for the biofilms of several strains.

The value of $R_{Biofilm}$ for each strain was obtained *via* conductivity measurements (Fig. 1) whereas the value of R_{ct}^{anode} for each strain was obtained *via* EIS measurements (Fig. 5 and 6). EIS measurements of charge transfer resistance demonstrated that strains that produced biofilms with higher conductivity also had lower R_{ct}^{anode} values (Fig. 5B). A likely explanation for this lower value is that electrons reaching the biofilm/anode interface after traveling through a biofilm with lower resistance will have greater energy than electrons transported through biofilms of higher resistance, therefore lowering the activation energy barrier for electron transfer to the anode. Thus, higher biofilm conductivity can lower the internal resistance by contributing a lower

Published on 16 January 2012 on http://pubs.rsc.org | doi:10.1039/C2EE03388G
Downloaded by University of Massachusetts - Amherst on 12 March 2013

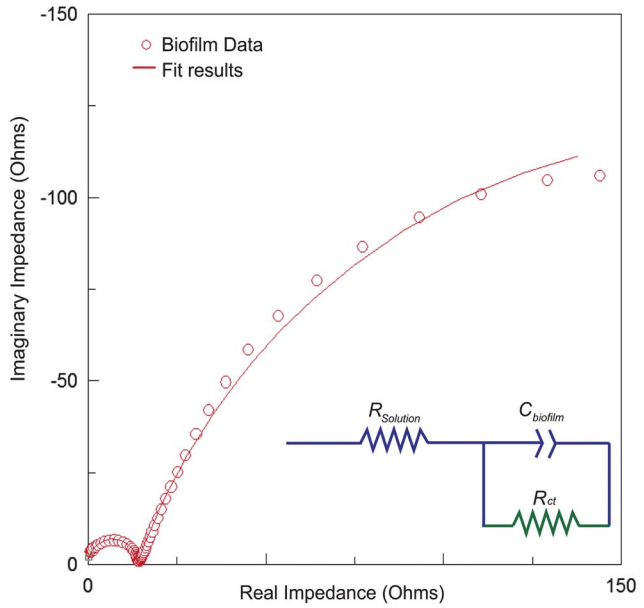

Fig. 6 Representative impedance spectrum for anode biofilm and fitting results obtained using electrochemical impedance spectroscopy (EIS). Inset: Equivalent circuit model used to extract EIS parameters.

R_{ct}^{anode} as well as lower $R_{Biofilm}$. However, the relative magnitude of $R_{Biofilm}$ is substantially more because the electrons in the biofilm need to travel over substantial distances to reach the anode and the resistance associated with long-distance electron transport is substantially higher than the resistance associated with the single electron transfer step from the biofilm to the anode at the biofilm/anode interface.

Additional verification of biofilm conductivity

The estimates of each of the resistance components that contribute to the overall internal resistance make it feasible to independently check the estimates for $R_{Biofilm}$ determined from the transport measurements initially used to determine biofilm conductivity. For example, for strain DL-1, plugging in the values for all other measured resistances into eqn (1) and (2) yields an estimate for $R_{Biofilm}$ of 874 ± 277 Ω, which compares favorably with the $R_{Biofilm}$ of 1208 ± 85 Ω obtained from the conductivity measurements.

Thus, EIS experiments independently confirm the biofilm conductivity value obtained *via* transport measurements and demonstrate the central role played by biofilm conductivity in electricity generation.

Factors other than biofilm conductivity influence current production

Making the assumption that the biofilm conductivity was the only limiting factor for the net current density, theoretical studies[16,17] described the relationship between current density (j) and biofilm conductivity ($\sigma_{biofilm}$) with Ohm's law:

$$j = -\sigma_{biofilm}\frac{(E_{OM} - E_{interface})}{\Delta z} \quad (3)$$

where, Δz in the distance over which electrons are transported, E_{OM} is the potential at which the electrons released by the microorganism through the outer membrane (OM) and $E_{interface}$ is the potential across the biofilm/anode interface.

There was a linear relationship between current density and biofilm conductivity for the strains of DL-1, that had lower biofilm conductivities, but strain KN400, which had the highest current density, did not produce as much current as would be predicted from the same linear relationship (Fig. 7).

This result demonstrates that as biofilm conductivity increases, other factors may begin to limit current production. Mass transfer limitations, which become increasingly important at high current densities,[22,27] is a likely explanation. Computational modeling[16] has suggested that electron donor mass transfer resistance becomes significant at higher biofilm conductivity. Furthermore, higher current production increases the release of protons into the biofilm and lower pH, resulting from the rates of proton flux that are too slow, may be a major factor limiting the current production.[17,29–31] Therefore, in order to achieve higher current densities, large biofilm conductivity is necessary but not the only requirement. Design improvements are also needed to reduce the electron donor mass transfer resistance as well as to address the issue of proton gradient. Novel electrode designs using ultramicroelectrodes might be an effective strategy to address these limitations.[18,19]

Experimental

Bacterial strains and culture conditions

Geobacter sulfurreducens strain DL-1 (ATCC 51573),[4] strain KN400,[4] and strain BEST[23] were obtained from our laboratory collection. The cultures were maintained under strictly anaerobic conditions in growth medium supplemented with fumarate (40 mM) as the electron acceptor with acetate (10 mM) as the electron donor as described previously.[3]

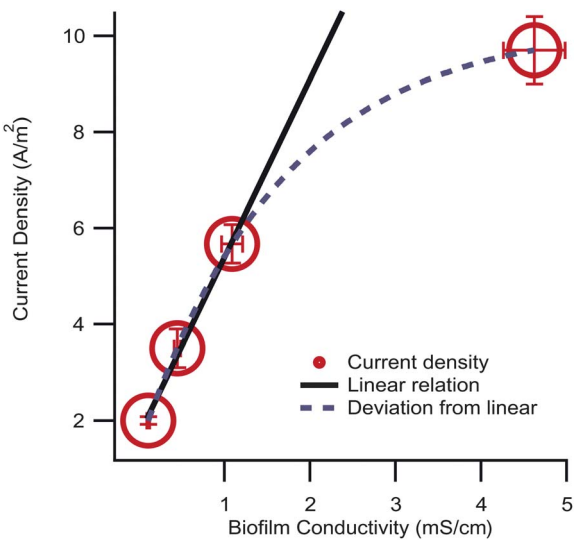

Fig. 7 Deviation from linear behavior between the biofilm conductivity and the MFC current density. Values represent mean ± standard deviation for biological replicates.

This journal is © The Royal Society of Chemistry 2012

Published on 16 January 2012 on http://pubs.rsc.org | doi:10.1039/C2EE03388G
Downloaded by University of Massachusetts - Amherst on 12 March 2013

The microbial fuel cell and conductivity measurement setup

The split-gold anodes were fabricated as described previously.[9] Glass slides (2.54 cm × 2.54 cm) were cleaned ultrasonically using successive rinses of trichloroethylene, acetone, and methanol and then blown dry with nitrogen. To achieve an insulating gap in the anode, a 50 μm or 100 μm diameter tungsten wire was placed on the glass substrate as a deposition mask. For four-probe measurements, electrodes were fabricated using standard photolithography processing. A 40 nm Au film atop a 10 nm Cr adhesion layer was thermally evaporated on these substrates, at 10^{-6} mbar, using a deposition rate 0.1 nm s^{-1}, thus producing gold split electrodes with a 50 μm or 100 μm non-conductive spacing. Optical microscopy revealed that the gap was uniform, and resistance measurements assured that the electrodes were well insulated from each other with $G_{gap} < 10^{-10}$ S. Both the sides of the split-anode were connected to cathode to promote biofilm growth on the anodes and to bridge the non-conductive gap. To measure either biofilm conductivity or charge transfer resistances, the connection between anode and cathode was removed and split-anodes were connected to the electronics (Fig. 5A). The reference electrode was Ag/AgCl.[9]

DC biofilm conductivity measurements

After disconnecting the split-anode from the cathode, when the open circuit potential of the anode became stable, biofilm conductivity was measured with a source meter (Keithley 2400) by applying either a small voltage across the split-anodes for two-probe measurements or a small current for four-probe measurements as described previously.[9] For four-probe measurements, an additional high-impedance voltmeter (Keithley 2000) was used to record the output voltage of the current source to calculate conductance.[9,32] For two-probe measurements, a voltage ramp of 0–0.05 V was applied across split electrodes in steps of 0.025 V. For each measurement, after allowing the exponential decay of the transient ionic current, the steady-state electronic current for each voltage was measured every second over a minimum period of 100 s using a Labview data acquisition program (National Instruments). Time-averaged current for each applied voltage was calculated to create the current–voltage (I–V) characteristics. For 4-probe measurements, a fixed current was applied between outer of the four electrodes and to measure the potential drop between two inner electrodes,[9,32] by measuring the voltage for each current every second over a period of 100 s, after reaching the steady-state. For both two and four-probe measurements, linearity of I–V characteristics was maintained by applying appropriate low voltage or current. The dissipative power was kept under 10^{-6} W to eliminate self-heating effects.

Confocal microscopy and biofilm thickness measurements

Biofilms were examined with confocal laser scanning microscopy (CLSM) as described previously.[3,13] Biofilms were stained with the LIVE/DEAD BacLight Bacterial Viability Kit (L7012) (Molecular Probes, Eugene, OR) following manufacturer's instructions. Anode biofilms were imaged with a Leica TCS SP5 microscope (Leica Microsystems GmbH, Wetzlar, Germany) with a HCX APO 63x (numerical aperture: 0.9) objective and a minimum of 5 fields of were imaged. Images were processed and analyzed with LAS AF software (Leica). A minimum of 5 random CLSM image stacks were used to determine average biofilm thickness using the biofilm analysis software Phobia Laser scanning microscopy Imaging Processor (PHLIP).[33] Thicknesses of biofilm of strains KN400, BEST, DL-1 and fumarate DL-1 were 40 μm, 60 μm, 50 μm and 130 μm respectively.

Biofilm conductivity calculation

In our previous studies, we have reported the biofilm conductivity of several strains using two-probe measurements.[9] Here we report the biofilm conductivity using four-probe measurements, which eliminate the possible contribution of contact resistance and electrode polarization (Ref. 9 and references therein). Biofilm conductivity (σ) was calculated from the measured conductance (G) using conformal mapping (the Schwarz-Christoffel transformation)[34] as described previously[9] using the following relation:

$$\sigma = G\frac{\pi}{L}\Big/\ln\left(\frac{8g}{\pi a}\right) \quad (4)$$

where L is the length of the electrodes ($L \approx 2.54$ cm); a is the half-spacing between the electrodes ($2a \approx 50$ μm) and g is the biofilm thickness measured using confocal microscopy. Above formula is valid for the limiting case $a < g \ll b$ where b is the half-width of the electrodes ($2b \approx 2.54$ cm). The proportionality coefficient between the conductivity measured using four-probe and two-probe methods, which accounts for contact resistance and electrode polarization,[32,35] was computed by measuring biofilm conductivity of strain KN400 as described previously.[9] Since four-probe and two-probe conductivities are always proportional,[32,35] the proportionality coefficient was used to estimate four-probe conductivity of biofilms of other strains from the measured two-probe conductivity.

Measurement of fuel cell current density

In order to accurately determine the maximum current density of the fuel cell, a non-cathode-limited fuel cell configuration was employed.[4] The cathode is an essential part of the overall redox system, because the electrons delivered to the anode by the bacteria must be utilized elsewhere in the fuel-cell. For a cathode reaction $Fe(CN)_6^{3-} + e^- = Fe(CN)_6^{4-}$, the electrochemical reduction must take place on the surface of the electrode. Clearly, the rate at which this reduction reaction happens will be proportional to the area of the electrode.[22] Therefore, if the total current is limited by cathode area, it will not reveal the true maximum possible current density. In the setup used to measure *in situ* conductivity, the anode and cathode area were equal, which limited maximum current due to a limiting cathode reaction. Therefore, a non-cathode limited fuel cell[4] was used to accurately determine the current density. In this setup, 3 mm diameter graphite rod was used as the anode with effective area 7×10^{-6} m^2. The cathode was a 2.54 cm × 2.54 cm sized carbon cloth with effective area 19.2×10^{-4} m^2. This area calculation was performed with a confocal microscope by measuring the diameter and the thread count of the carbon fibers.[10] Since the

Downloaded by University of Massachusetts - Amherst on 12 March 2013
Published on 16 January 2012 on http://pubs.rsc.org | doi:10.1039/C2EE03388G

cathode area is 275 times larger than anode, the cathode reaction is no longer a limiting factor. Fuel cell current density was calculated by dividing the steady-state current by the area of the graphite rod.

Electrochemical impedance spectroscopy (EIS)

Electrochemical impedance spectroscopy (EIS) was performed using a Solartron 1252/1287 impedance analyzer. For anode impedance spectra, split electrodes were externally short circuited and an impedance spectrum of the biofilm-electrolyte interface was measured using the three-electrode cell with anode as the working electrode (WE) and the cathode as the counter electrode (CE) (Fig. 5A). For cathode impedance spectra, the cathode served as the WE and the anode as the CE. An Ag/AgCl electrode in the working electrode chamber was used as a reference electrode (RE). When EIS measurements were performed on the entire fuel cell, the anode was used as the WE and the cathode was used as the RE as well as the CE.[24,28]

EIS measurements were carried out in a frequency range of 300 kHz to 100 mHz with an ac signal of 0.1 V amplitude. Charge transfer resistance values were extracted using equivalent circuit of a single time constant model (Fig. 6 inset) in which solution resistance ($R_{solution}$) is in series with parallel combination of capacitance ($C_{biofilm}$) and charge transfer resistance (R_{ct}).[26,28] Data fitting was performed with ZView software (Scribner Inc.) which uses LEVM algorithm developed by J. Ross Macdonald.[37] Anode potentials were continuously monitored with an Ag/AgCl reference electrode in the anode chamber. For all impedance measurements, open circuit potential was monitored until it reached a constant value before over imposing an ac signal. All comparisons among strains were made with the lowest values of charge transfer resistance and biofilm resistance measured at the open circuit potential.

EIS measurements allowed evaluation of kinetic parameters of the biofilm (charge transfer resistance, exchange current density and activation overpotential) by fitting a one-time constant model to the impedance spectra (Fig. 6).[28,36] The relationship between the charge transfer resistance and the exchange current is given by:[26]

$$R_{ct} = \frac{RT}{nFi_0} \quad (5)$$

where i_0 is the exchange current which is given as:

$$i_0 = FAk^0[C]^{\alpha}_{bulk}[C]^{1-\alpha}_{bulk} \quad (6)$$

where k^0 is the standard rate constant, α is the transfer coefficient and C is the concentration. The deviation of potential (E) from the equilibrium potential (E_e) is termed as overpotential (or polarization).

$$\eta = E - E_e \quad (7)$$

Eqn (6) is valid only for small η. For processes that have a small value of i_0, a high overpotential is required to induce current flow. When i_0 is large, little or no applied overpotential is required to drive the reaction. Thus, activation overpotential is a measure for the slowness of the reaction.[27]

Measurements of protein content in the biofilm

In order to compare the reported electron transfer rate per mg protein to that computed from conductivity measurements, the protein content of the biofilm was measured as described previously.[9] The biofilms were removed from the gold electrodes using 600 μl isotonic wash buffer. Collected biomass was immediately frozen with liquid nitrogen and stored at −20 °C. After thawing, vortexing, sonicating, and centrifuging for 5 min at 9000 RPM, supernatants and pellets (cell debris) were collected. Supernatant protein concentration was measured by Quick Start Bradford Dye Reagent (BioRad, CA, USA). Standards were prepared by using Bovine Serum Albumin (Sigma, Mo, USA). Pellets were suspended in 200 μl deionised water and boiled with 0.5% SDS for 10 min and protein concentration was determined by the bicinchoninic acid method with bovine serum albumin as a standard as described previously.[4] Since a confluent biofilm with uniform thickness was formed over the electrodes spanning a non-conductive gap, the protein content in the gap was estimated by using total protein per electrode area and multiplying it by the gap area.

Scanning electron microscopy (SEM)

Gold electrodes with the grown biofilms were removed from the anode chamber of MFC and biofilms were fixed with 1% gluteraldehyde and 1% formaldehyde. Biofilms were dehydrated with graded ethanol series (30, 50, 70, 80, 95, and 100%) for 10 min each step with a gentle periodic agitation. Then, the biofilms were CO_2 critical-point dried from ethanol transitional solvent with a 3-hour slow, continuous exchange. For SEM imaging, the biofilms were sputter coated in a Polaron E-5100 Sputter Coater (2 min at 2.2 kV) with argon at 13 Pa by using a gold target and observed in a JEOL JSM-5400 SEM with an accelerating voltage of 5 kV.

Conclusions

These studies demonstrate that microbial strains with higher biofilm conductivities produce higher current densities and that this can be attributed not only to reduced resistance to electron flow through the biofilm, but also to a lower activation energy barrier for electron transfer between the biofilm and the anode. These findings help resolve the previous uncertainty over the relationship between biofilm conductivity and the capacity for current production that arose due to indirect inference of biofilm conductivity, rather than direct measurements. With the method for simultaneously measuring biofilm conductivity and potential losses described here it should be possible to evaluate the conductivity of current-producing biofilms of other pure culture cultures or mixed microbial communities in order to gain further insight into the role of biofilm conductivity in promoting current production in microbial fuel cells or microbe-electrode electron exchange in cathodic processes[37] such as microbial electrosynthesis[38,39] or hydrogen production.[40]

Biofilm conductivity appears to be an integral part of electron transport for current production and higher biofilm conductivity facilitates enhanced rates of extracellular electron transfer. Therefore, even though biofilm conductivity is not the only factor limiting the net current production, further increasing the

 This journal is © The Royal Society of Chemistry 2012

Published on 16 January 2012 on http://pubs.rsc.org | doi:10.1039/C2EE03388G
Downloaded by University of Massachusetts - Amherst on 12 March 2013

conductivity of microbial biofilms might represent an effective strategy to enhance the current density of microbial fuel cells if other factors limiting current production can be effectively managed.

The increase in current density associated with increased biofilm conductivity is consistent with well-known responses of abiotic catalysts.[22] However, living biofilms are unique in that the properties of the catalytic layer rapidly change in response to an alteration in environmental conditions or other manipulations that influence gene expression. For example, simple environmental variables, such as temperature, can influence the production of the conductive pili,[8,41,42] that are responsible for electron transport through the biofilms of *G. sulfurreducens*.[9,13] The dynamic nature of biofilms and other properties, such as their ability to function as supercapacitors,[43] offers unique possibilities for bioelectronics applications.

Acknowledgements

We thank Dale Callaham and Ashley Franks for SEM and confocal imaging of biofilms. This research was supported by the Office of Naval Research (grant no.N00014-10-1-0084), the Office of Science (BER), US Department of Energy (award no. DE-SC0004114 and Cooperative Agreement no. DE-FC02-02ER63446) as well as the NSF Center for Hierarchical Manufacturing (grant no. CMMI-1025020).

References

1 D. R. Lovley, *Nat. Rev. Microbiol.*, 2006, **4**, 497–508.
2 B. Logan, *Nat. Rev. Microbiol.*, 2009, **7**, 375–381.
3 K. P. Nevin, H. Richter, S. F. Covalla, J. P. Johnson, T. L. Woodard, A. L. Orloff, H. Jia, M. Zhang and D. R. Lovley, *Environ. Microbiol.*, 2008, **10**, 2505–2514.
4 H. Yi, K. P. Nevin, B. C. Kim, A. E. Franks, A. Klimes, L. M. Tender and D. R. Lovley, *Biosens. Bioelectron.*, 2009, **24**, 3498–3503.
5 D. R. Lovley and K. P. Nevin, *Curr. Opin. Biotechnol.*, 2011, **22**, 441–448.
6 P. D. Kiely, J. M. Regan and B. E. Logan, *Curr. Opin. Biotechnol.*, 2011, **22**, 378–385.
7 D. R. Lovley, T. Ueki, T. Zhang, N. S. Malvankar, P. M. Shrestha, K. Flanagan, M. Aklujkar, J. E. Butler, L. Giloteaux, A. E. Rotaru, D. E. Holmes, A. E. Franks, R. Orellana, C. Risso and K. P. Nevin, *Adv. Microb. Physiol.*, 2011, **59**, 1–100.
8 K. P. Nevin, B. C. Kim, R. H. Glaven, J. P. Johnson, T. L. Woodard, B. A. Methé, R. J. DiDonato Jr, S. F. Covalla, A. E. Franks, A. Liu and D. R. Lovley, *PLoS One*, 2009, **4**, e5628.
9 N. S. Malvankar, M. Vargas, K. P. Nevin, A. E. Franks, C. Leang, B.-C. Kim, K. Inoue, T. Mester, S. F. Covalla, J. P. Johnson, V. M. Rotello, M. T. Tuominen and D. R. Lovley, *Nat. Nanotechnol.*, 2011, **6**, 573–579.
10 H. Richter, K. P. Nevin, H. Jia, D. A. Lowy, D. R. Lovley and L. M. Tender, *Energy Environ. Sci.*, 2009, **2**, 506–516.
11 S. M. Strycharz-Glaven, R. M. Snider, A. Guiseppi-Elie and L. M. Tender, *Energy Environ. Sci.*, 2011, **4**, 4366–4379.
12 N. S. Malvankar, M. T. Tuominen and D. R. Lovley, *Energy & Environmental Science*, 2012, DOI: 10.1039/c2ee02613a.
13 G. Reguera, K. P. Nevin, J. S. Nicoll, S. F. Covalla, T. L. Woodard and D. R. Lovley, *Appl. Environ. Microbiol.*, 2006, **72**, 7345–7348.
14 M. Morita, N. S. Malvankar, A. E. Franks, Z. M. Summers, L. Giloteaux, A. E. Rotaru, C. Rotaru and D. R. Lovley, *mBio*, 2011, **2**, e00159-11.
15 N. S. Malvankar, J. Lou, A. E. Franks, M. T. Tuominen and D. R. Lovley, *Manuscript in preparation*.
16 A. K. Marcus, C. I. Torres and B. E. Rittmann, *Biotechnol. Bioeng.*, 2007, **98**, 1171–1182.
17 C. I. Torres, A. K. Marcus, H. S. Lee, P. Parameswaran, R. Krajmalnik-Brown and B. E. Rittmann, *FEMS Microbiol. Rev.*, 2009, **34**, 3–17.
18 D. Pocaznoi, B. Erable, M.-L. Delia and A. Bergel, *Energy Environ. Sci.*, 2012, **5**, 5287–5296.
19 Y. Liu, H. Kim, R. Franklin and D. R. Bond, *Energy Environ. Sci.*, 2010, **3**, 1782–1788.
20 C. I. Torres, A. K. Marcus, P. Parameswaran and B. E. Rittmann, *Environ. Sci. Technol.*, 2008, **42**, 6593–6597.
21 D. Schrott Germán, B. P. Sebastian, R. Luciana, E.-N. Abraham and J. Pablo Busalmen, *Electrochim. Acta*, 2011, **56**, 10791–10795.
22 A. Dicks and J. Larminie, *Fuel cell systems explained*, John Wiley & Sons, 2000.
23 J. W. Voordeckers, B.-C. Kim, M. Izallalen and D. R. Lovley, *Appl. Environ. Microbiol.*, 2010, **76**, 2371–2375.
24 E. Marsili, J. Sun and D. R. Bond, *Electroanalysis*, 2010, **22**, 865–874.
25 A. Esteve Núñez, M. Rothermich, M. Sharma and D. Lovley, *Environ. Microbiol.*, 2005, **7**, 641–648.
26 K. Rabaey and W. Verstraete, *Trends Biotechnol.*, 2005, **23**, 291–298.
27 K. Rabaey, L. Angenent, U. Schröder and J. Keller, *Bioelectrochemical Systems: From Extracellular Electron Transfer to Biotechnological Application*, Intl Water Assn, 2009.
28 A. K. Manohar, O. Bretschger, K. H. Nealson and F. Mansfeld, *Bioelectrochemistry*, 2008, **72**, 149–154.
29 C. I. Torres, A. Kato Marcus and B. E. Rittmann, *Biotechnol. Bioeng.*, 2008, **100**, 872–881.
30 A. E. Franks, K. P. Nevin, H. Jia, M. Izallalen, T. L. Woodard and D. R. Lovley, *Energy Environ. Sci.*, 2009, **2**, 113–119.
31 A. K. Marcus, C. I. Torres and B. E. Rittmann, *Bioresour. Technol.*, 2011, **102**, 253–262.
32 U. Lange and V. M. Mirsky, *J. Electroanal. Chem.*, 2008, **622**, 246–251.
33 L. Mueller, J. de Brouwer, J. Almeida, L. Stal and J. Xavier, *BMC Ecol.*, 2006, **6**, 1.
34 J. Kankare and E. L. Kupila, *J. Electroanal. Chem.*, 1992, **322**, 167–181.
35 Q. Hao, V. Kulikov and V. M. Mirsky, *Sens. Actuators, B*, 2003, **94**, 352–357.
36 E. Barsoukov and J. R. Macdonald, *Impedance Spectroscopy: Theory, Experiment and Applications*. 2nd ed., John Wiley and Sons Inc., New Jersey, 2005.
37 D. R. Lovley, *Environ. Microbiol. Rep.*, 2011, **3**, 27–35.
38 K. P. Nevin, T. L. Woodard, A. E. Franks, Z. M. Summers and D. R. Lovley, *mBio*, 2010, **1**, e00103-10.
39 K. P. Nevin, S. A. Hensley, A. E. Franks, Z. M. Summers, J. H. Ou, T. L. Woodard, O. L. Snoeyenbos-West and D. R. Lovley, *Appl. Environ. Microbiol.*, 2011, **77**, 2882–2886.
40 J. S. Geelhoed and A. J. M. Stams, *Environ. Sci. Technol.*, 2011, **45**, 815–820.
41 S. E. Childers, S. Ciufo and D. R. Lovley, *Nature*, 2002, **416**, 767–769.
42 G. Reguera, K. D. McCarthy, T. Mehta, J. S. Nicoll, M. T. Tuominen and D. R. Lovley, *Nature*, 2005, **435**, 1098–1101.
43 N. S. Malvankar, T. Mester, M. T. Tuominen and D. R. Lovley, *ChemPhysChem*, 2012, DOI: 10.1002/cphc.201100865.